Energy Reports 7 (2021) 6438–6450

Contents lists available at ScienceDirect

Energy Reports

journal homepage: www.elsevier.com/locate/egyr

Research paper

Flexural modes coupling in cantilever-type piezoelectric energy harvesters

Abdolreza Pasharavesh [a,b], Hamid Dalir [b,*]

[a] School of Mechanical Engineering, Purdue University, West Lafayette, IN, USA
[b] Department of Mechanical and Energy Engineering, Purdue School of Engineering and Technology, Indianapolis, IN, USA

ARTICLE INFO

Article history:
Received 10 May 2021
Received in revised form 4 September 2021
Accepted 24 September 2021
Available online 7 October 2021

Keywords:
Micro power generation
Cantilever-type harvester
Piezoelectric laminated beam
Nonlinear vibration
Flexural modes coupling

ABSTRACT

The ability to harness the waste mechanical energy and convert it into useful electrical power has made kinetic energy harvesters a promising candidate to provide an everlasting energy source for wireless autonomous devices. Nonlinearities, whether introduced deliberately for the sake of bandwidth broadening or present intrinsically, can highly influence the dynamic response and output power behavior of these type of energy scavengers. This paper aims to investigate the effect of nonlinearity on multi-mode vibrational response of a harvester composed of a cantilevered piezoelectric composite beam with an attached mass of finite dimensions. To that end, first of all a 3-DoF lumped parameter coupled electromechanical model of the device is developed through a comprehensive mathematical approach and its mode shapes and natural frequencies are calculated. The perturbation method of multiple scales is then applied to obtain the steady state solutions to the extracted order-reduced governing equations of the system. Results indicate that a harvester with a cubic attached mass exhibits a simple Duffing-type resonance as the excitation frequency falls in the vicinity of each natural frequency. That occurs while for a U-shaped mass the vibration modes would be coupled through occurrence of an internal resonance. In this latter case, both flexural modes of the piezoelectric beam are stimulated by a single frequency excitation and contribute to the power generation leading to an enhancement of the total output power which is the major advantage of the proposed design in this paper compared to the other existing energy harvesters. The frequency response curves of the output power are found to be composed of four branches and include Hopf bifurcations and instability regions. To verify the results obtained from the analytical approach, they are compared to a numerical solution where a good agreement is observed between them.

1. Introduction

Realizing ambient power supplies which are able to collect different types of waste energy from the surrounding environment and convert them into electrical form in order to provide an everlasting controlled source of electrical power is the main objective of energy harvesting technology. Achieving this goal has been an ambition of mankind since the emergence of applications which require energy-autonomous electronic devices including wireless sensor networks (WSNs) (Yu et al., 2014), implantable medical devices (IMDs) (Miao et al., 2006), and radio frequency identification systems (RFIDs) (Hande et al., 2009), to name but a few. Kinetic energy stored in the small amplitude vibrations of civil structures, industrial machinery, or even human's body has long shown to be a promising ambient source of energy. Kinetic energy scavengers generally employ a resonating structure whose energy is converted into the electrical power through either of piezoelectric (Chung and Lee, 2014), electromagnetic (Wang et al., 2009), or electrostatic (Sheu et al., 2011) transduction mechanisms.

In the linear regime, resonant harvesters exhibit a sharp peak in their output power frequency curve which restricts energy harvesting to a very narrow bandwidth in the neighborhood of their natural frequencies. To overcome this challenge, nonlinear harvesters with either deliberately introduced or inherent nonlinearities, have been widely employed (Quinn et al., 2011; Pasharavesh et al., 2020a; Green et al., 2013). They benefit the bending of their resonance curves to generate reasonable amounts of power in a wider range of excitation frequencies. However, the coexistence of low- and high-energy stable equilibria in the nonlinear frequency response is the main drawback of nonlinear systems which makes their wideband operation dependent to the trajectory of the excitation. It is because in an uncontrolled Duffing resonator the response may either converge to high- or low-energy steady-state which differ to a large extent in power generation potential. Therefore, the enhancement of useful bandwidth only occurs in the case that the response lies on the upper

* Corresponding author.
E-mail address: hdalir@purdue.edu (H. Dalir).

https://doi.org/10.1016/j.egyr.2021.09.109

branch of the frequency response curve (Mann and Sims, 2009; Pasharavesh et al., 2020b). As a result, in order that a nonlinear electromechanical resonator be able to effectively be employed as a wideband energy harvester in different environments, a control mechanism should exist to guarantee the convergence of the system to the desired response under all conditions. Several researchers have proposed strategies to guarantee that the output power of nonlinear harvesters surfs the high-energy branch of the response curve (Mallick et al., 2016; Masuda and Sato, 2016). These approaches generally use a mechanical (Zhou et al., 2015) or electrical (Pasharavesh and Ahmadian, 2020) perturbation to trigger the response to jump from the low to the high energy equilibrium point. Thanks to these efforts and achievements nonlinear resonators have become the first choice of researchers wherever bandwidth broadening is a concern in the design of kinetic energy harvesters (Hu et al., 2017). However, it should be noted that as a matter of fact, the performance of nonlinear harvesters in broadening the bandwidth of energy generation is a function of their excitation amplitude. A slightly excited nonlinear system behaves almost similar to its linear counterpart and the nonlinear effects are exhibited only at sufficiently large excitations. Therefore, the average amplitude of the existing ambient vibration plays a key role in the design process of such systems and a harvester designed for a specific application may not be expected to offer the same performance when used in a different environment. In addition, this limitation of nonlinear harvesters usually impels the designer to make a trade-off between the generated power and effective bandwidth to achieve a system which best suits the overall system requirements.

The nonlinear behavior in a piezoelectric harvester occurs due to either material nonlinearity (Stanton et al., 2010), geometrical nonlinearity (Pasharavesh and Ahmadian, 2018), or integration to nonlinear circuits of energy harvesting (Singh et al., 2015). Hajati and Kim fabricated the first ultra-wide bandwidth piezoelectric nonlinear MEMS harvester which employed the midplane stretching effect in a micro-scale doubly-clamped beam resulting in an amplitude-stiffened Duffing resonance (Hajati and Kim, 2011). The serious problem of their design was its high natural frequency preventing the harvester from capturing the energy stored in ambient vibrations which are generally of low-frequency. A similar nonlinear behavior is observed in cantilevered harvesters due to the combined effect of both nonlinear curvature and inertia (Pasharavesh et al., 2017). That occurs while the natural frequencies of the cantilever design are generally much lower than the doubly-clamped one which makes them more efficient choices. Surveying the existing literature on fabrication of piezoelectric generators reveals that most of the fabricated devices compromise large attached tip masses with dimensions comparable with or even larger than the beam length. This necessitates taking into account the effect of the tip mass offset together with its rotary inertia in their modeling which has been done by several researchers (Lumentut and Howard, 2016, 2017; Pasharavesh et al., 2019).

There are several examples of previous researches which have carried out a modal analysis of cantilever piezoelectric bimorphs and have exploited the results in multi-mode linear simulation of the harvester. Jiang et al. derived a set of mode shapes for a piezoelectric bimorph with an attached tip mass and utilized them to analyze the vibratory behavior of the harvester (Jiang et al., 2005). Erturk and Inman implemented the mode summation method and performed a detailed study on the cantilevered piezoelectric harvesters using the Euler–Bernoulli, Rayleigh, and Timoshenko beam theories (Erturk and Inman, 2008; Erturk, 2012). Pasharavesh et al. brought into account the damping effect due to extracting electrical energy from the device and conducted a complex modal analysis (Pasharavesh et al., 2019). Unlike the linear case, to avoid the involved cumbersome formulation in multi-mode nonlinear models, most researchers have preferred to adopt their approximate single-mode counterparts (Panyam and Daqaq, 2016; Masana and Daqaq, 2011). Although, this approximation can lead to somehow accurate results for systems with distant natural frequencies, the contribution of higher modes to the generated power grows considerably as their corresponding frequencies approach that of the first mode. It occurs mainly due to the larger electromechanical coupling parameters associated with the higher modes of vibration. In addition, the nonlinear coupling of the flexural modes through occurrence of the internal resonances can highly alter the frequency response of the system and give rise to behaviors which cannot be predicted using a single-mode model.

In the present paper, the nonlinear coupling of vibrational modes in a kinetic harvester composed of a piezoelectric bimorph with an attached tip mass is studied and its effect on the output power behavior of the device is evaluated. A 3-Dof electromechanically coupled nonlinear model of the device is derived and analyzed employing the perturbation method of multiple scales. The needed condition for the occurrence of an internal resonance is extracted as the geometric shape of the attached mass varies. Additionally, the contribution of the second mode to the power generation and the effect of mode coupling on the frequency response of the harvester are investigated. A numerical solution to the governing equations is carried out as well whose results are employed to verify the analytical findings.

2. Modeling and formulation

As indicated by its name, a cantilever-type harvester employs a clamped-free beam with an attached tip mass as the vibratory element. The attached mass experiences a fictitious inertial force when the clamped end of the beam is periodically displaced. If the frequency of the applied displacement is in the vicinity of one of the natural frequencies of the system, the amplitude of vibration would considerably grow. This amplitude increase continues up to the point at which the input mechanical power to the system equals the harvested electrical power plus mechanical losses. The mechanism by which the energy transduction from the mechanical to the electrical domain occurs may differ from one harvester to another. Some harvesters employ magnetic induction phenomena through relative motion of a permanent magnet and a coil to perform the energy conversion. In some others, separation of opposite charges stored on the beam and a conductive fixed substrate when the vibrating beam recedes from the substrate is responsible for the conversion. Another widely used energy conversion mechanism employs the piezoelectric effect in electroelastic materials to bridge between mechanical and electrical domains. This latter method has shown to be a promising candidate thanks to its high conversion efficiency and low fabrication complexity. Although in this paper the formulations are derived for a piezoelectric beam, similar equations may be used to simulate the behavior of electromagnetic and electrostatic harvesters, as well.

The schematic view of a piezoelectric cantilever-type harvester is demonstrated in Fig. 1. As can be seen in this figure the beam is composed of a middle base layer of thickness $2h_B$ sandwiched between two identical layers of piezoelectric material with thickness h_P. The beam is supposed to have a constant width of b. To extract the electrical energy stored in the piezoelectric layers, each layer should be covered by two conductive electrodes from both sides. In the figure shown, since the base layer is supposed to be conductive, only one electrode layer is placed on the free surface of each piezoelectric layer. As depicted in the figure, these electrodes are of length L_e which is not necessarily

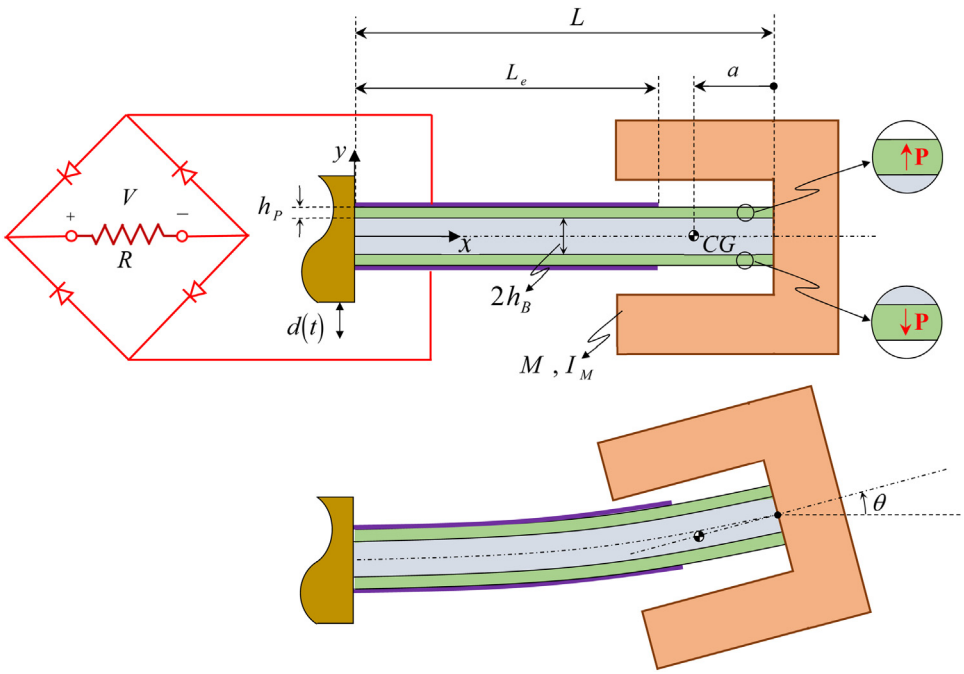

Fig. 1. Schematic view of a cantilever-type piezoelectric harvester with an attached U-shaped mass.

equal to the beam length L. Therefore, as long as $L_e < L$ the piezoelectric layers are only partially covered by the electrodes. The generated voltages of the piezoelectric layers are added up to the total voltage measured at the output terminals of the harvester through connection of the electrodes in a series fashion. To do that the piezoelectric layers must both be polarized along thickness but in opposite directions. It should be noted that the output voltage of the harvester is proportional to integral of the beam's curvature over the length covered by the electrodes. This integral is approximately equal to the slope difference between the start and end points of the electrode. Therefore, assuming that the electrode begins from the fixed end of the beam (which has a zero slope), in order to harvest the maximum energy, it must end at a point with maximum slope according to the dominant vibrational mode of the beam.

One important characteristic of the device which may considerably affect its dynamic response is the location of the center of gravity of the attached mass. For a lumped mass the center of gravity coincides the intersection point of the neutral axis and the cross section of the beam at its free end ($a = 0$, where a as shown in the figure is the distance of the center of gravity denoted by CG from the beam's free end). For a cubic mass of finite dimensions (attached symmetrically with respect to the neutral axis) the center of gravity falls on the neutral axis and to the right of the free end of the beam ($a < 0$). That occurs while for a U-shaped mass (the case shown in the figure), the center of gravity can fall to the left hand of the beam's free end ($a > 0$). For $a \neq 0$ the translational acceleration of the attached mass depends not only on the linear acceleration of the beam's free end but also to its rotational acceleration. In this case, the sign of a determines how CG moves as the beam's free end rotates in a way that the counter-clockwise rotation of the beam cross section at its free end leads to downward and upward displacements of CG for $a > 0$ and $a < 0$, respectively. In this paper, a comprehensive study is carried out by letting a to adopt either of negative, zero, or positive values. Attached masses of cubic shape are normally used in most of energy harvesters to bring their first natural frequency down into the frequency range of ambient vibrations. However, the second natural frequency highly grows in harvesters with cubic masses preventing them from harvesting energy through multi-mode vibrations in environments with varying frequency or wide-band excitations. That occurs while, for a U-shaped mass the ratio of these two natural frequencies can be kept low which can lead to nonlinear coupling of the modes through internal resonances, as will be shown later in this paper. Briefly speaking this is the main reason behind the idea of using the U-shaped mass and occurs since the inertial force and moment applied by an attached mass of this shape to the beam act in opposite directions.

Fig. 2 depicts an infinitesimal longitudinal element of the beam together with all forces and moments acting on it. The employed coordinate system is similar to the one in Fig. 1 with x axis along the beam's neutral axis in undeformed position, and y axis along the lateral direction. The equilibrium of the moments with respect to the z direction and forces with respect to the x and y directions, result in:

$$\begin{cases} M_3' + F_2 = M_{iz} & (a) \\ (F_1 \cos\theta)' - (F_2 \sin\theta)' = f_{ix} & (b) \\ (F_1 \sin\theta)' + (F_2 \cos\theta)' + q_f = f_{iy} & (c) \end{cases} \tag{1}$$

where as shown in the figure, θ denotes the rotation angle of the element and M_3 represents the total moment in z direction acting on the cross section of the beam. Also F_1 and F_2 are the equivalent forces acting along normal and tangent directions with respect to the beam's cross section. In addition, M_{iz}, f_{ix}, and f_{iy} denote the inertial distributed momentum and forces acting on the beam, which by representing the longitudinal and lateral displacements respectively by u and v, may be written as follows:

$$\begin{aligned} M_{iz} &= \left(I_G + Ma^2\right)\ddot{\theta}\,\delta\,(x-L) && (a) \\ f_{ix} &= m\ddot{u} + M\,(u + a\,(1-\cos\theta))^{\cdot\cdot}\,\delta\,(x-L) \\ &= m\ddot{u} + M\left(\ddot{u} + a\ddot{\theta}\sin\theta + a\dot{\theta}^2\cos\theta\right)\delta\,(x-L) && (b) \\ f_{iy} &= m\ddot{v} + M\,(v - a\sin\theta)^{\cdot\cdot}\,\delta\,(x-L) \\ &= m\ddot{v} + M\left(\ddot{v} - a\ddot{\theta}\cos\theta + a\dot{\theta}^2\sin\theta\right)\delta\,(x-L) && (c) \end{aligned} \tag{2}$$

In the above expressions M and I_G respectively denote the total mass and moment of inertia about the center of gravity of the

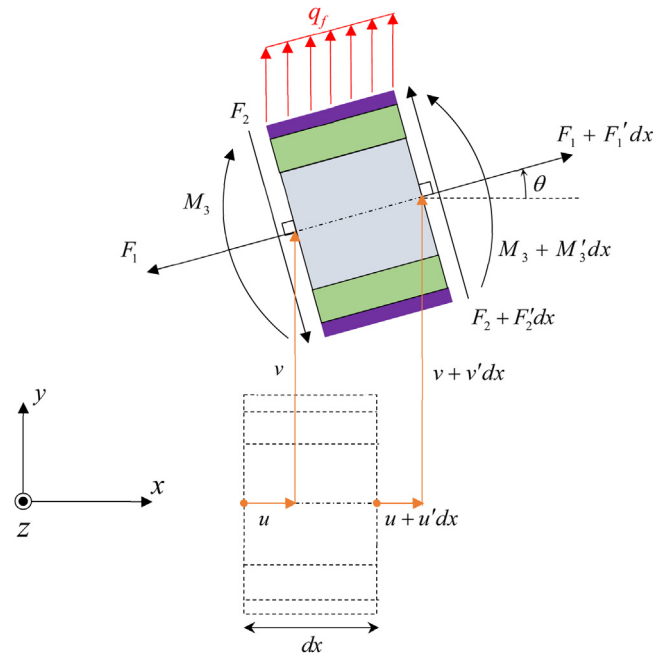

Fig. 2. An infinitesimal element of the beam before and after deflection.

attached mass. Introducing the radius of gyration r_G the moment of inertia may be written as $I_G = M{r_G}^2$. Furthermore, m in Eq. (2) designates the mass per unit length of the beam:

$$m = 2b\left(h_B\rho_B + h_P\rho_P\right) \tag{3}$$

with ρ_B and ρ_P denoting the densities of the constituent materials of the base and the piezoelectric layers. It is noteworthy that in derivation of Eq. (2)-a, according to Euler–Bernoulli assumption for beams of small thicknesses the effect of the beam's rotary inertia has been neglected.

Integrating Eq. (2)-b with respect to x from L to x noting that $F_1\cos\theta - F_2\sin\theta$ vanishes at $x = L$ (the free end of the beam), results in:

$$F_1 = \frac{1}{\cos\theta}\left[F_2\sin\theta + \int_L^x f_{ix}dx\right] \tag{4}$$

Since no external force is applied to the beam along the longitudinal direction, according to inextensionality condition the following relation holds between u and v (Mahmoodi et al., 2008):

$$u = \int_0^x \left(\sqrt{1 - v'^2} - 1\right)dx \tag{5}$$

Substituting Eqs. (2), (4), and (5), into (1), the partial differential equation governing the lateral vibrations of the beam is derived as:

$$\left(\left(I_G + Ma^2\right)\delta\left(x - L\right)\ddot{\theta} - \frac{M_3'}{\cos\theta} + \left(\int_L^x \left[\begin{array}{l}\left(m + M\delta\left(x - L\right)\right)\left(\int_0^x \left(\sqrt{1 - v'^2} - 1\right)^{\cdot\cdot} dx\right) \\ +M\left(a\ddot{\theta}\sin\theta + a\dot{\theta}^2\cos\theta\right)\delta\left(x - L\right)\end{array}\right]dx\right) \times \tan\theta\right)' + q_f = m\ddot{v} + M\left(\ddot{v} - a\ddot{\theta}\cos\theta + a\dot{\theta}^2\sin\theta\right)\delta\left(x - L\right) \tag{6}$$

where q_f is the summation of the damping force and the fictitious force arising in a frame attached to the clamped end of the beam whose displacement is denoted by $d(t)$ as shown in Fig. 1:

$$q_f\left(x, t\right) = -c\dot{v} - \left(m + M\delta\left(x - L\right) + Ma\delta'\left(x - L\right)\right)\ddot{d}\left(t\right) \tag{7}$$

The above expression is derived by calculating a system of force and couple acting at the free end of the beam which is equivalent to the fictitious force passing through the center of gravity of the attached mass. Acceleration $\ddot{d}(t)$ is supposed to be a single harmonic function with amplitude A and frequency Ω:

$$\ddot{d}\left(t\right) = A\cos\left(\Omega t\right) \tag{8}$$

From Fig. 2 the rotation angle θ may be written as a function of the derivatives of the displacement components as:

$$\theta = \tan^{-1}\left(\frac{v'}{1 + u'}\right) \tag{9}$$

where the prime superscript denotes differentiation with respect to x. Substituting Eq. (5) into the above relation, then using the Taylor series expansion one obtains:

$$\begin{aligned} &\theta = v' + \frac{1}{6}v'^3 + \text{H.O.T.}, \qquad \sin\theta = v', \\ &\cos\theta = 1 - \frac{1}{2}v'^2 + \text{H.O.T.}, \qquad \tan\theta = v' + \frac{1}{2}v'^3 + \text{H.O.T.} \end{aligned} \tag{10}$$

where H.O.T. stands for the nonlinear terms of higher orders.

The constitutive equations of the piezoelectric layers are (Yang, 2005):

$$\begin{aligned} &T_1 = c_{11}^E S_1 - e_{21}E_2 \quad (a) \\ &D_2 = e_{21}S_1 + \varepsilon_{22}^S E_2 \quad (b) \end{aligned} \tag{11}$$

in which **T**, **S**, **E**, and **D** represent stress, strain, electric field, and electric displacement vectors, respectively. Also, **c**, **ε**, and **e** designate the matrices containing elastic, dielectric, and piezoelectric constants of the material (The E and S superscripts determine whether the coefficients are measured under constant electric field or strain condition). Indices 1 and 2 in this equation are associated with axes x and y, respectively. The axial strain in an Euler–Bernoulli beam may be written as:

$$S_1 = -y\theta' \tag{12}$$

where y denotes the distance of the point at which the strain is calculated from the neutral axis. Substituting the above expression into Eq. (11)-b, one obtains:

$$E_2 = \frac{D_2 \pm e_{21}y\theta'}{\varepsilon_{22}^S} \tag{13}$$

It should be noted that in the above equation and all other equations which follow, wherever a plus-minus or a minus-plus sign is used, it means that the upper sign must be used for the upper layer of piezoelectric, while the lower one is used for the lower layer. Since as mentioned before the piezoelectric layers are assumed to be polarized in opposite directions, their transverse piezoelectric constant will be of opposite sign leading to the appearance of the plus-minus sign in Eq. (13).

If the output voltage of the harvester is denoted by V, due to symmetry the voltage difference across each piezoelectric layer would be equal to $V/2$. By definition the voltage difference between any two points of the space can be derived by integration of the electric field over an arbitrary path which starts from one of

those points and ends at the other one. Therefore, integrating the relation given in Eq. (13) for the electric field along the thickness of the piezoelectric layers, one obtains:

$$\frac{V}{2} = \mp \int_{\pm h_B}^{\pm(h_B+h_P)} E_2 dy = \mp \int_{\pm h_B}^{\pm(h_B+h_P)} \frac{D_2 \pm e_{21} y\theta'}{\varepsilon_{22}^S} dy$$
$$= -\frac{h_P}{\varepsilon_{22}^S}\left[D_2 + e_{21}\left(h_B + \frac{h_P}{2}\right)\theta'\right] \tag{14}$$

from which D_2 may be calculated as:

$$D_2 = -\left[\frac{\varepsilon_{22}^S}{2h_P}V + e_{21}\left(h_B + \frac{h_P}{2}\right)\theta'\right]\Pi\left(\frac{x}{L_e} - \frac{1}{2}\right) \tag{15}$$

where $\Pi(x)$ represents the rectangular function:

$$\Pi(x) = \begin{cases} 1, & -1/2 < x < 1/2 \\ 0, & \text{otherwise} \end{cases} \tag{16}$$

Substituting Eq. (15) into (13), one obtains:

$$E_2 = \frac{-\left[\frac{\varepsilon_{22}^S}{2h_P}V + e_{21}\left(h_B + \frac{h_P}{2}\right)\theta'\right]\Pi\left(\frac{x}{L_e} - \frac{1}{2}\right) \pm e_{21} y\theta'}{\varepsilon_{22}^S} \tag{17}$$

which after substitution into Eq. (11)-a gives the following expression for the axial stress in the piezoelectric layers:

$$T_1 = -\left(c_{11}^E + \frac{{e_{21}}^2}{\varepsilon_{22}^S}\right) y\theta' \pm \left(\frac{{e_{21}}^2}{\varepsilon_{22}^S}\left(h_B + \frac{h_P}{2}\right)\theta' + \frac{e_{21}}{2h_P}V\right)$$
$$\times\ \Pi\left(\frac{x}{L_e} - \frac{1}{2}\right) \tag{18}$$

For the base layer the stress may be simply derived using the Hooke's law as:

$$T_1 = -E_y y\theta' \tag{19}$$

where E_y designates the effective Young's modulus of the base material. Using the above expressions derived for the axial stresses within the base and piezoelectric layers, one can calculate the bending moment in the beam as:

$$M_3 = -b\int_{-h_B-h_P}^{h_B+h_P} T_1 y dy$$
$$= D\theta' - \left[2b\int_{h_B}^{h_B+h_P}\left(\frac{{e_{21}}^2}{\varepsilon_{22}^S}\left(h_B + \frac{h_P}{2}\right)\theta' + \frac{e_{21}}{2h_P}V\right) y dy\right]$$
$$\times\ \Pi\left(\frac{x}{L_e} - \frac{1}{2}\right) \tag{20}$$

where D is the bending stiffness of the laminated composite beam:

$$D = b\int_{-h_B}^{h_B} E_y y^2 dy + 2b\int_{h_B}^{h_B+h_P}\left(c_{11}^E + \frac{{e_{21}}^2}{\varepsilon_{22}^S}\right) y^2 dy \tag{21}$$

It is noteworthy that in derivation of Eq. (20) the effect of electrodes' stiffness on the mechanical properties of the system is assumed as negligible which is reasonable since their thicknesses are commonly chosen to be very thin.

Finally, substituting Eqs. (7), (10), and (20) into (6), the governing equation of the system is found to be:

$$m\ddot{v} - \left(I_G + Ma^2\right)\left(\ddot{v}'\delta(x-L)\right)' + M\left(\ddot{v} - a\ddot{v}'\right)\delta(x-L) + c\dot{v}$$
$$+D\left(v''' + v'^2 v''' + v' v''^2\right)' + \frac{1}{2}\left(v'\int_L^x\left[m\left(\int_0^x v'^2 dx\right)^{\cdot\cdot}\right]dx\right)' =$$
$$+\left(\left[2b\int_{h_B}^{h_B+h_P}\left(\frac{{e_{21}}^2}{\varepsilon_{22}^S}\left(h_B + \frac{h_P}{2}\right)v'' + \frac{e_{21}}{2h_P}V\right) y dy\right]\right.$$
$$\left.\times\ \Pi\left(\frac{x}{L_e} - \frac{1}{2}\right)\right)'' - Mv''\left(-\frac{1}{2}\left(\int_0^L v'^2 dx\right)^{\cdot\cdot} + a\left(\dot{v}'v'\right)^{\cdot}\Big|_{x=L}\right)$$
$$-\left(m + M\delta(x-L) + Ma\delta'(x-L)\right)\ddot{d}(t) \tag{22}$$

with the boundary conditions similar to those of a simple Euler–Bernoulli clamped-free beam. To solve the above equation for v, one first needs to find another equation governing the output voltage of the harvester V. This second equation may be found by relating the total charge stored on the electrodes, the output terminal voltage, and their time derivatives through the impedance of the connected load. Integrating equation (21) in accordance to Gauss' law over the surface of piezoelectric layers covered by the electrodes gives the total stored charge q on each electrode, which for the upper electrode results in:

$$q = \frac{bL_e\varepsilon_{22}^S}{2h_P}V + be_{21}\left(h_B + \frac{h_P}{2}\right)v'\Big|_{x=L_e} \tag{23}$$

Assuming the external load connected to the output terminals of the harvester to be a pure resistance R, the following relation is obtained by the use of Ohm's law:

$$V + R\dot{q} = 0 \tag{24}$$

Substituting q from Eq. (23) into the above relation, another differential equation relating the terminal voltage V to the deflection v is found as:

$$V + R\left(\frac{bL_e\varepsilon_{22}^S}{2h_P}\dot{V} + be_{21}\left(h_B + \frac{h_P}{2}\right)\dot{v}'\Big|_{x=L_e}\right) = 0 \tag{25}$$

3. Semi-analytical solution

To find the output voltage of the harvester and consequently its total harvested power, one needs to simultaneously solve the coupled differential equations given in Eqs. (22) and (25). In this section, the perturbative method of multiple scales is employed to derive a semi-analytical solution to these equations. To investigate how mode coupling phenomena affects the behavior of the device and how the solution found by a single-mode approximation is corrected by involving the second vibration mode of the beam, first using a two mode approximation the lateral deflection of the beam is written as:

$$v(x,t) = \eta(t)\phi(x) + \xi(t)\psi(x) \tag{26}$$

ϕ and ψ in the above expression are the first and second mode shapes of an Euler–Bernoulli cantilever beam (Rao, 2007):

$$\alpha(x) = (\cos\beta_\alpha x - \cosh\beta_\alpha x) - \frac{\cos\beta_\alpha L + \cosh\beta_\alpha L}{\sin\beta_\alpha L + \sinh\beta_\alpha L}$$
$$\times\ (\sin\beta_\alpha x - \sinh\beta_\alpha x) \qquad \alpha = \phi, \psi \tag{27}$$

where:

$$\beta_\phi L = 1.8751, \qquad \beta_\psi L = 4.6941 \tag{28}$$

The ordinary differential equations governing the vibrations of the beam at its first two modes are then found by applying the Galerkin decomposition method to the PDE of Eq. (22). To do that,

first the approximate solution given in Eq. (26) is substituted into the PDE and then the equation is multiplied by the mode shapes and integrated with respect to x along the beam length. Following this procedure results in the below set of ODEs:

$$\begin{cases} m_{11}\ddot{\eta} + m_{12}\ddot{\xi} + k_{11}\eta + k_{12}\xi = \alpha_{11}\eta^3 + \alpha_{12}\eta^2\xi + \alpha_{13}\eta\xi^2 \\ \quad +\alpha_{14}\xi^3 + \alpha_{15}\eta^2\ddot{\eta} + \alpha_{16}\eta^2\ddot{\xi} + \alpha_{17}\ddot{\eta}\xi^2 + \alpha_{18}\xi^2\ddot{\xi} + \alpha_{19}\eta\dot{\eta}^2 \\ \quad +\alpha_{110}\eta\dot{\xi}^2 + \alpha_{111}\dot{\eta}^2\xi + \alpha_{112}\xi\dot{\xi}^2 + \alpha_{113}\eta\dot{\eta}\dot{\xi} + \alpha_{114}\dot{\eta}\xi\dot{\xi} \\ \quad +\alpha_{115}\eta\ddot{\eta}\xi + \alpha_{116}\eta\xi\ddot{\xi} - \hat{\mu}_1\dot{\eta} + \hat{\chi}_1 V + K_1\cos(\Omega t) \\ m_{21}\ddot{\xi} + m_{22}\ddot{\eta} + k_{21}\xi + k_{22}\eta = \alpha_{21}\xi^3 + \alpha_{22}\xi^2\eta + \alpha_{23}\xi\eta^2 \\ \quad +\alpha_{24}\eta^3 + \alpha_{25}\xi^2\ddot{\xi} + \alpha_{26}\xi^2\ddot{\eta} + \alpha_{27}\ddot{\xi}\eta^2 + \alpha_{28}\eta^2\ddot{\eta} + \alpha_{29}\xi\dot{\xi}^2 \\ \quad +\alpha_{210}\xi\dot{\eta}^2 + \alpha_{211}\dot{\xi}^2\eta + \alpha_{212}\eta\dot{\eta}^2 + \alpha_{213}\xi\dot{\xi}\dot{\eta} + \alpha_{214}\dot{\xi}\eta\dot{\eta} \\ \quad +\alpha_{215}\xi\ddot{\xi}\eta + \alpha_{216}\xi\eta\ddot{\eta} - \hat{\mu}_2\dot{\xi} + \hat{\chi}_2 V + K_2\cos(\Omega t) \end{cases} \tag{29}$$

where the electromechanical coupling parameters ($\hat{\chi}_i$s), the elements of the mass and stiffness matrices and the force vector (m_{ij}s, k_{ij}s, and K_is), and the damping coefficients ($\hat{\mu}_i$s), are as follows:

$$\begin{aligned} m_{i1} &= m\int_0^L \lambda_i{}^2 dx + \left(I_G + Ma^2\right)\left(\lambda_i'^2\right)\Big|_{x=L} + M\left(\lambda_i{}^2 - a\lambda_i'\lambda_i\right)\Big|_{x=L} \\ m_{i2} &= \left(I_G + Ma^2\right)\left(\lambda_i'\mu_i'\right)\Big|_{x=L} + M\left(\mu_i\lambda_i - a\mu_i'\lambda_i\right)\Big|_{x=L} \\ k_{i1} &= \int_0^L \left(D - \frac{2be_{21}{}^2 h_P}{\varepsilon_{22}^S}\left(h_B + \frac{h_P}{2}\right)^2 \times \Pi\left(\frac{x}{L_e} - \frac{1}{2}\right)\right)\lambda_i''^2 dx, \qquad \begin{matrix} i = 1,2 \\ \lambda_1 = \mu_2 = \phi \\ \lambda_2 = \mu_1 = \psi \end{matrix} \\ k_{i2} &= \int_0^L \left(D - \frac{2be_{21}{}^2 h_P}{\varepsilon_{22}^S}\left(h_B + \frac{h_P}{2}\right)^2 \Pi\left(\frac{x}{L_e} - \frac{1}{2}\right)\right)\lambda_i''\mu_i'' dx \\ \hat{\chi}_i &= be_{21}\left(h_B + \frac{h_P}{2}\right)\lambda_i'\big|_{x=L_e}, \qquad \hat{\mu}_i = c\int_0^L \lambda_i{}^2 dx, \\ K_i &= -\left(m\int_0^L \lambda_i dx + M\,\lambda_i|_{x=L} - Ma\,\lambda_i'\big|_{x=L}\right)A \end{aligned} \tag{30}$$

Also the coefficients of the nonlinear terms (α_{ij}s) are as presented in Appendix A.

The third governing ODE of the harvester is found by substitution of Eq. (26) into (25) as:

$$V + R\left(C_P\dot{V} + \hat{\chi}_1\dot{\eta} + \hat{\chi}_2\dot{\xi}\right) = 0 \tag{31}$$

where C_P is the equivalent capacitance of the piezoelectric layers:

$$C_P = \frac{bL_e\varepsilon_{22}^S}{2h_P} \tag{32}$$

To solve Eqs. (29) and (31) by multiple scales method first by considering $T_0 = t$ and $T_2 = \varepsilon^2 t$, where ε is a small dimensionless parameter, the voltage V and the modal deflections η and ξ are expanded as the following power series:

$$\eta = \varepsilon^1\eta_1 + \varepsilon^2\eta_2 + \varepsilon^2\eta_3 + \cdots, \qquad \xi = \varepsilon^1\xi_1 + \varepsilon^2\xi_2 + \varepsilon^2\xi_3 + \cdots, \\ V = \varepsilon^1 V_1 + \varepsilon^2 V_2 + \varepsilon^2 V_3 + \cdots \tag{33}$$

The electromechanical coupling parameters and modal damping coefficients are supposed to be of order ε and ε^2, respectively. Also, the excitation is supposed to be of order ε^3. Therefore:

$$\hat{\chi}_i = \varepsilon\chi_i, \qquad \hat{\mu}_i = \varepsilon^2\mu_i, \qquad K_i = \varepsilon^3 k_i \qquad i = 1,2 \tag{34}$$

The above assumptions guarantee that the terms are ordered so that the excitation terms and the terms associated with damping, whether mechanical damping or damping due to energy harvesting, appear simultaneously with the highest order of nonlinearity.

For a 2DoF third order nonlinear oscillatory system, the internal resonance occurs if the second natural frequency is approximately three times the first one. The natural frequencies of a cantilever beam do not meet this criterion but as will be shown later using the U-shaped attached mass one can adjust the frequencies so that this relation holds. Also assuming that the excitation frequency is in the vicinity of the first natural frequency, introducing the detuning parameters σ_1 and σ_2, one can write:

$$\Omega = \omega_1 + \varepsilon^2\sigma_1, \qquad \omega_2 = 3\omega_1 + \varepsilon^2\sigma_2 \tag{35}$$

Substituting Eqs. (33) to (35) into (29) and (31) then separating the terms of different powers of ε, one obtains the following sets of equations:

$$\varepsilon^1: \begin{cases} m_{11}D_0^2\eta_1 + m_{12}D_0^2\xi_1 + k_{11}\eta_1 + k_{12}\xi_1 = 0 \\ m_{21}D_0^2\xi_1 + m_{22}D_0^2\eta_1 + k_{21}\xi_1 + k_{22}\eta_1 = 0 \\ V_1 + RC_PD_0V_1 = 0 \end{cases} \tag{a}$$

$$\varepsilon^2: \begin{cases} m_{11}D_0^2\eta_2 + m_{12}D_0^2\xi_2 + k_{11}\eta + k_{12}\xi = \chi_1 V_1 \\ m_{21}D_0^2\xi_2 + m_{22}D_0^2\eta_2 + k_{21}\xi + k_{22}\eta = \chi_2 V_1 \\ V_2 + R\left(C_PD_0V_2 + \chi_1D_0\eta_1 + \chi_2D_0\xi_1\right) = 0 \end{cases} \tag{b}$$

$$\varepsilon^3: \begin{cases} m_{11}D_0^2\eta_3 + m_{12}D_0^2\xi_3 + k_{11}\eta_3 + k_{12}\xi_3 = f_1 \\ m_{21}D_0^2\xi_3 + m_{22}D_0^2\eta_3 + k_{21}\xi_3 + k_{22}\eta_3 = f_2 \\ V_3 + R\left(C_P\left(D_0V_3 + D_2V_1\right) + \chi_1D_0\eta_2 + \chi_2D_0\xi_2\right) = 0 \end{cases} \tag{c}$$

(36)

where:

$$\begin{aligned} f_1 &= -2m_{11}D_0D_2\eta_1 - 2m_{12}D_0D_2\xi_1 + \alpha_{11}\eta_1^3 + \alpha_{12}\eta_1^2\xi_1 \\ &\quad +\alpha_{13}\eta_1\xi_1^2 + \alpha_{14}\xi_1^3 + \alpha_{15}\eta_1^2D_0^2\eta_1 + \alpha_{16}\eta_1{}^2D_0^2\xi_1 \\ &\quad +\alpha_{17}\xi_1{}^2D_0^2\eta_1 + \alpha_{18}\xi_1{}^2D_0^2\xi_1 + \alpha_{19}\eta_1\left(D_0\eta_1\right)^2 + \alpha_{110}\eta_1\left(D_0\xi_1\right)^2 \\ &\quad +\alpha_{111}\left(D_0\eta_1\right)^2\xi_1 + \alpha_{112}\xi_1\left(D_0\xi_1\right)^2 \\ &\quad +\alpha_{113}\eta_1\left(D_0\eta_1\right)\left(D_0\xi_1\right) + \alpha_{114}\left(D_0\eta_1\right)\xi_1\left(D_0\xi_1\right) \\ &\quad +\alpha_{115}\eta_1\xi_1D_0^2\eta_1 \\ &\quad +\alpha_{116}\eta_1\xi_1D_0^2\xi_1 - \mu_1D_0\eta_1 + \chi_1V_2 + k_1\cos(\Omega t) \\ f_2 &= -2m_{21}D_0D_2\xi_1 - 2m_{22}D_0D_2\eta_1 + \alpha_{21}\xi_1^3 + \alpha_{22}\xi_1^2\eta_1 \\ &\quad +\alpha_{23}\xi_1\eta_1^2 + \alpha_{24}\eta_1^3 + \alpha_{25}\xi_1^2D_0^2\xi_1 + \alpha_{26}\xi_1^2D_0^2\eta_1 \\ &\quad +\alpha_{27}\eta_1^2D_0^2\xi_1 + \alpha_{28}\eta_1^2D_0^2\eta_1 + \alpha_{29}\xi_1\left(D_0\xi_1\right)^2 + \alpha_{210}\xi_1\left(D_0\eta_1\right)^2 \\ &\quad +\alpha_{211}\left(D_0\xi_1\right)^2\eta_1 + \alpha_{212}\eta_1\left(D_0\eta_1\right)^2 \\ &\quad +\alpha_{213}\xi_1\left(D_0\xi_1\right)\left(D_0\eta_1\right) + \alpha_{214}\left(D_0\xi_1\right)\eta_1\left(D_0\eta_1\right) \\ &\quad +\alpha_{215}\xi_1\eta_1D_0^2\xi_1 \\ &\quad +\alpha_{216}\xi_1\eta_1D_0^2\eta_1 - \mu_2D_0\xi_1 + \chi_2V_2 + k_2\cos(\Omega t) \end{aligned} \tag{37}$$

D_is in the above two equations denote partial derivatives with respect to T_is. The solution of Eq. (36)-a can be written as:

$$\begin{aligned}\eta_1 &= A_1 \exp(i\omega_1 T_0) + A_2 \exp(i\omega_2 T_0) + \text{cc}\\ \xi_1 &= \alpha_1 A_1 \exp(i\omega_1 T_0) + \alpha_2 A_2 \exp(i\omega_2 T_0) + \text{cc}\\ V_1 &= 0\end{aligned} \tag{38}$$

where:

$$\alpha_i = -\frac{k_{11} - m_{11}\omega_i^2}{k_{12} - m_{12}\omega_i^2} \qquad i = 1, 2 \tag{39}$$

In Eq. (38), "cc" stands for the complex conjugate terms. Also ω_1 and ω_2 are the first two natural frequencies of the harvester calculated from the following characteristic equation:

$$\begin{aligned}&(m_{11}m_{21} - m_{22}m_{12})\,\omega^4 + (k_{12}m_{22} + k_{22}m_{12} - k_{11}m_{21} - k_{21}m_{11})\\ &\quad\times\ \omega^2 + k_{11}k_{21} - k_{22}k_{12} = 0\end{aligned} \tag{40}$$

Substituting Eq. (38) into (36)-(b), the solution is obtained as:

$$\begin{aligned}&\eta_2 = \xi_2 = 0,\\ &V_2 = -\frac{\chi_1 + \alpha_1\chi_2}{1 + iRC_P\omega_1} Ri\omega_1 A_1 \exp(i\omega_1 T_0)\\ &\quad - \frac{\chi_1 + \alpha_2\chi_2}{1 + iRC_P\omega_2} Ri\omega_2 A_2 \exp(i\omega_2 T_0) + cc\end{aligned} \tag{41}$$

To eliminate the secular terms in Eq. (36)-c, the coefficients of the term $\exp(i\omega_i T_0)$ in the following expressions must vanish:

$$\beta_i f_1 + f_2 \tag{42}$$

where:

$$\beta_i = -\frac{k_{22} - m_{22}\omega_i^2}{k_{11} - m_{11}\omega_i^2}, \qquad i = 1, 2 \tag{43}$$

Consequently, after substituting Eqs. (38) and (41) into (42), the solvability conditions for Eq. (36)-c are derived as:

$$\begin{cases}2\left(\beta_1(m_{11} + m_{12}\alpha_1) + (m_{21}\alpha_1 + m_{22})\right) i\omega_1 A_1'\\ \quad + \left((\beta_1\mu_1 + \alpha_1\mu_2) + \dfrac{(\beta_1\chi_1 + \chi_2)(\chi_1 + \alpha_1\chi_2)}{1 + iRC_P\omega_1} R\right) i\omega_1 A_1 =\\ c_{11}{A_1}^2\bar{A}_1 + c_{12}A_1A_2\bar{A}_2 + c_{13}{\bar{A}_1}^2 A_2 \exp(i\sigma_2 T_0)\\ \quad + \dfrac{1}{2}(\beta_1 k_1 + k_2)\exp(i\sigma_1 T_0)\\ 2\left(\beta_2(m_{11} + m_{12}\alpha_2) + (m_{21}\alpha_2 + m_{22})\right) i\omega_2 A_2'\\ \quad + \left((\beta_2\mu_1 + \alpha_2\mu_2) + \dfrac{(\beta_2\chi_1 + \chi_2)(\chi_1 + \alpha_2\chi_2)}{1 + iRC_P\omega_2} R\right) i\omega_2 A_2 =\\ c_{21}{A_2}^2\bar{A}_2 + c_{22}A_1\bar{A}_1A_2 + c_{23}{A_1}^3 \exp(-i\sigma_2 T_0)\end{cases} \tag{44}$$

where the coefficients c_{ij}s are as given in Appendix B.

Replacing A_1 and A_2 in the above equation by the following polar representations:

$$A_1 = \frac{1}{2}a_1 e^{i(\sigma_1 T_2 - \gamma_1)}, \qquad A_2 = \frac{1}{2}a_2 e^{i((3\sigma_1 - \sigma_2)T_2 - 3\gamma_1 + \gamma_2)} \tag{45}$$

then separating the real and imaginary parts of the equations, results in the following 4-DoF first order autonomous system whose equilibrium points correspond to steady state vibrational responses of the device:

$$\begin{aligned}a_1' &= -\left(\mu_1^{mech} + \mu_1^{elec}\right)a_1 + \frac{c_{13}{a_1}^2 a_2 \sin(\gamma_2) + 4k\sin(\gamma_1)}{8m_1\omega_1}\\ \gamma_1' &= \sigma_1 - \Delta\omega_1\\ &\quad + \frac{c_{11}{a_1}^3 + c_{12}a_1a_2^2 + c_{13}{a_1}^2 a_2\cos(\gamma_2) + 4k\cos(\gamma_1)}{8m_1\omega_1 a_1}\\ a_2' &= -\left(\mu_2^{mech} + \mu_2^{elec}\right)a_2 - \frac{c_{23}{a_1}^3\sin(\gamma_2)}{8m_2\omega_2}\\ \gamma_2' &= \sigma_2 + \Delta\omega_2 - 3\Delta\omega_1\\ &\quad + 3\frac{c_{11}{a_1}^3 + c_{12}a_1{a_2}^2 + c_{13}{a_1}^2 a_2\cos(\gamma_2) + 4k\cos(\gamma_1)}{8m_1\omega_1 a_1}\\ &\quad - \frac{c_{21}{a_2}^3 + c_{22}{a_1}^2 a_2 + c_{23}{a_1}^3\cos(\gamma_2)}{8m_2\omega_2 a_2}\end{aligned} \tag{46}$$

In the above equations μ_i^{mech} and μ_i^{elec} are mechanical and electrical modal damping coefficients associated with the ith mode, m_is are modal masses, and k is the modal force associated with the first mode. Also, $\Delta\omega_i$s designate the variation of the ith natural frequency due to electromechanical damping. The below equation shows how they are calculated from the previously introduced parameters:

$$\begin{aligned}&m_1 = \beta_1(m_{11} + m_{12}\alpha_1) + (m_{21}\alpha_1 + m_{22}),\\ &m_2 = \beta_2(m_{11} + m_{12}\alpha_2) + (m_{21}\alpha_2 + m_{22}), \qquad k = \beta_1 k_1 + k_2\\ &\mu_1^{mech} = \frac{(\beta_1\mu_1 + \alpha_1\mu_2)}{2m_1}, \qquad \mu_1^{elec} = \frac{(\beta_1\chi_1 + \chi_2)(\chi_1 + \alpha_1\chi_2)R}{2m_1\left(1 + R^2{C_P}^2{\omega_1}^2\right)}\\ &\mu_2^{mech} = \frac{(\beta_2\mu_1 + \alpha_2\mu_2)}{2m_2}, \qquad \mu_2^{elec} = \frac{(\beta_2\chi_1 + \chi_2)(\chi_1 + \alpha_2\chi_2)R}{2m_2\left(1 + R^2{C_P}^2{\omega_2}^2\right)}\\ &\Delta\omega_1 = \frac{(\beta_1\chi_1 + \chi_2)(\chi_1 + \alpha_1\chi_2)R^2 C_P\omega_1}{2m_1\left(1 + R^2{C_P}^2{\omega_1}^2\right)},\\ &\Delta\omega_2 = \frac{(\beta_2\chi_1 + \chi_2)(\chi_1 + \alpha_2\chi_2)R^2 C_P\omega_2}{2m_2\left(1 + R^2{C_P}^2{\omega_2}^2\right)}\end{aligned} \tag{47}$$

As can be seen in Eq. (41), due to the occurrence of internal resonance the output voltage of the harvester is composed of two harmonics. Therefore, the total average extracted power from the device will be the summation of powers associated with each harmonic as:

$$\bar{P}_{out} = \frac{(\chi_1 + \alpha_1\chi_2)^2}{2\left(1 + R^2{C_P}^2\omega_1^2\right)}R{\omega_1}^2{a_1}^2 + \frac{(\chi_1 + \alpha_2\chi_2)^2}{2\left(1 + R^2{C_P}^2{\omega_2}^2\right)}R{\omega_2}^2{a_2}^2 \tag{48}$$

4. Results and discussion

In this section, the already created model is used to explore how coupling of the flexural modes in a cantilever harvester affects its dynamic behavior and generated electrical power in both linear and nonlinear regimes. To do that first of all a small scale energy harvesting device composed of a piezoelectric laminated beam is considered as the case study. The harvester employs a 3-layer composite beam similar to what shown in Fig. 1 with a length of $L = 5$ mm and width of $b = 10$ mm as its main component. The thickness of the base layer is assumed to be $2h_B = 200\,\mu$m while each piezoelectric layer has a thickness of $h_P = 10\,\mu$m. The constituent materials of the base and piezoelectric layers are brass and PZT-5H, respectively, whose physical properties are given in Table 1. It is also assumed that the beam is completely covered by electrodes ($L_e = 5$ mm) and the damping coefficient is $c = 0.5$ N s. It should be noted that the maximum stress which occurs in the piezoelectric layer in

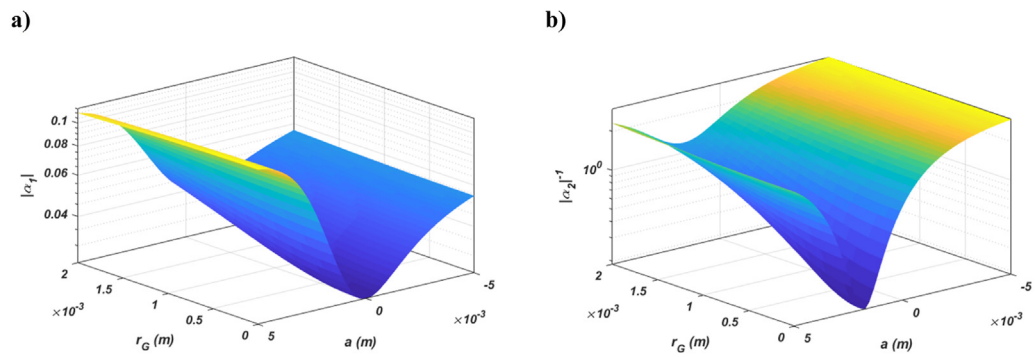

Fig. 3. Variation of (a) $|\alpha_1|$ and (b) $|\alpha_2|^{-1}$ with respect to the location of the center of gravity and the radius of gyration of the attached mass.

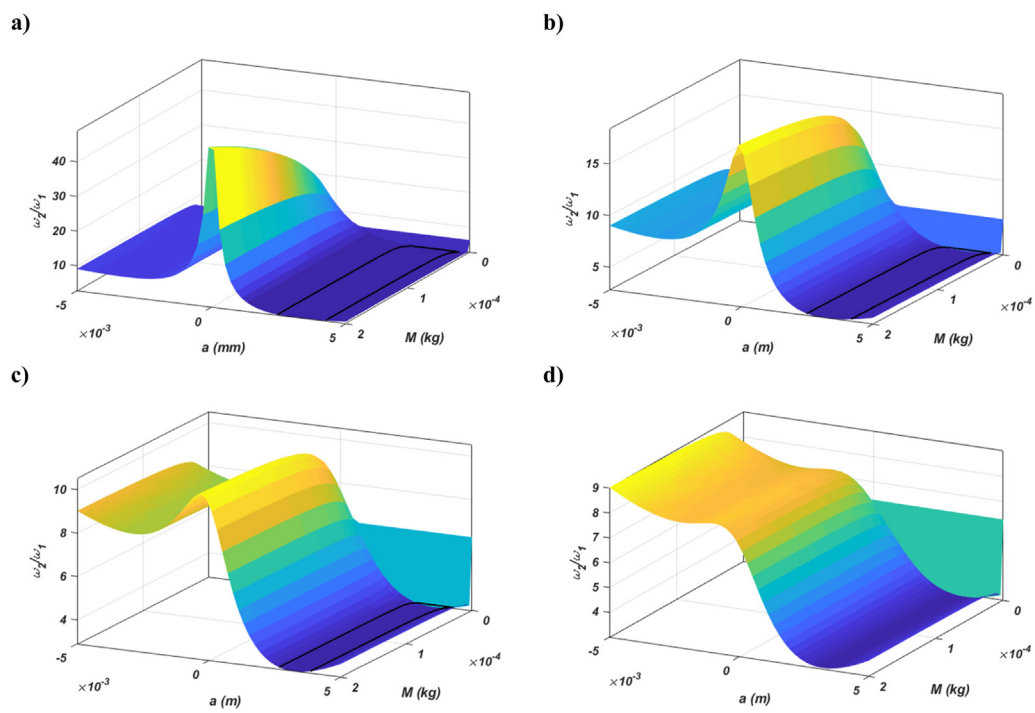

Fig. 4. Variation of the second to first natural frequency ratio with respect to the total mass and location of the center of gravity of the attached mass for (a) $r_G = 0$, (b) $r_G = 0.5$ mm, (c) $r_G = 1$ mm, and (d) $r_G = 1.5$ mm.

any arbitrary transverse section of the beam is a function of two quantities. First the curvature of the beam at that specific section due to the bending and second the total thickness of the beam (the summation of the base and piezoelectric layers thicknesses). While for beams of large thicknesses this maximum stress may exceed the failure limit of the structure as curvature increases, it remains in an acceptable range for thin beams even in large curvature regime. This condition is generally called "large curvature–small strain" in the literature. As can be seen for the selected dimensions above the length of the beam is about 25 times its thickness which guarantees that the maximum stress is in the safe region while the harvester operates in the nonlinear regime.

As the first step of our investigation, let us neglect the nonlinear terms in Eq. (29) and study the coupling effect in the linear regime. In the linearly approximated set of governing equations, the diagonal elements of the mass and stiffness matrices i.e. m_{12}, m_{21}, k_{12}, and k_{21} are responsible for the coupling. As a result, as long as these elements are nonzero on expects the vibration mode shapes of the device to be a combination of the mode shapes of the cantilever beam given in Eq. (27). As indicated by Eq. (38), the coefficients α_1 and α_2 can fully determine how the first two normal modes of a simple clamped-free beam combine to form the mode shapes of the harvester composed of the piezoelectric laminated beam and a tip mass of finite dimensions. For a device with no piezoelectric layer and no attached tip mass those diagonal elements all vanish resulting in $\alpha_1 = 1/\alpha_2 = 0$ which means that the mode shapes of the device are identical to ones given

Table 1
Physical parameters used in simulations.

Parameter	Brass	PZT-5H
Density ρ (kg/m^3)	8730	7500
Effective Young's modulus E_y (GPa)	100	–
Elastic coefficient c_{11} (GPa)	–	126
Piezoelectric coefficient e_{21} (C/m^2)	–	6.5
Dielectric coefficient ε_{22} (C/V m)	–	1.32×10^{-8}

in Eq. (27). Otherwise, one can easily derive the mode shapes by calculation of the coefficients α_1 and α_2 in accordance to Eq. (39). Enhancement of $|\alpha_1|$ and $|\alpha_2|$ respectively indicate an increase in participation of the second mode shape of the cantilever beam in the first and second mode shapes of the harvester. Therefore, as $|\alpha_1|$ and $|\alpha_2|^{-1}$ increase one can expect the mode shapes and consequently the natural frequencies of the device to further deviate from those of the cantilever beam. Fig. 3 demonstrates how these latter parameters vary as the radius of gyration r_G and the location of the center of gravity a change for a 200 mg attached mass. As can be seen in this figure, both $|\alpha_1|$ and $|\alpha_2|^{-1}$ show an almost similar behavior. As the radius of gyration increases both plots show an increase indicating a stronger coupling of the modes. Furthermore, as the center of gravity of the attached mass moves away from the free end of the beam whether to the right or left the coupling of the flexural modes increases. The significant difference is that $|\alpha_1|$ gets minimized when the center of gravity of the attached mass coincides the free end of the beam ($a \simeq 0$), while the same happens to $|\alpha_2|^{-1}$ at some positive value of a ($a \simeq 1.7$ mm).

When the mode shapes which are in fact the generalized eigenvectors of the stiffness and mass matrices vary, one expects the generalized eigenvalues (the squared of the natural frequencies) obtained from the characteristic Eq. (40) change as well. The ratio of the natural frequencies is a significant parameter which determines whether the vibration modes would be coupled in the nonlinear regime through an internal resonance or not. Fig. 4 depicts this ratio as a function of the total mass M and the location of the center of gravity a for four different values of the radius of gyration of the attached mass. In this figure, the case with zero radius of gyration corresponds to attached masses made of high density material whose dimensions and consequently radius of gyration may be neglected in comparison to the length of the beam. Since as evidenced by Eq. (29) the involved nonlinearity is of the third order, the occurrence of an internal resonance would be expected in the nonlinear regime if the ratio of the natural frequencies approximately equals 3. Due to this fact, the contour line corresponding to $\omega_2/\omega_1 = 3$ is depicted as well in all subplots of Fig. 4 (the solid black line). As can be seen, for $r_G = 2$ mm and higher the second natural frequency is larger than three times the first one for all values of M and a. Therefore, no internal resonance is possible to occur for that specific case up to the performed order of nonlinear approximation. Furthermore, since these contour lines only pass through the region with $a > 0$, for the nonlinear coupling of the flexural modes to occur the attached tip mass must be of the U-shaped form.

Now, let us turn our attention to the system's behavior in the nonlinear regime and consider a harvester for which the parameters of the attached mass are chosen to be in the vicinity of the contour line depicted in Fig. 4. The nonlinear frequency response curves in this section are plotted through continuation of the equilibria of the autonomous dynamical system given in Eq. (46) by using MatCont which is a toolbox in Matlab for continuation and bifurcation analysis implementing the pseudo-arclength continuation method. Calculations show that for a harvester with a $M = 200$ mg attached mass of $r_G = 0.5$ mm, the second natural frequency will be exactly three times the first one if a is chosen to be equal to 2.5 mm. Therefore, according to the definition of the detuning parameters given in Eq. (35), for such a system σ_2 can be continuously adjusted between negative, zero, and positive values through slightly changing a in the vicinity of the reference value $a = 2.5$ mm. Additionally, σ_1 may be controlled through sweeping the excitation frequency in the neighborhood of the first natural frequency of the harvester derived from Eq. (40) and is set as the continuation parameter to obtain the frequency–amplitude response curves.

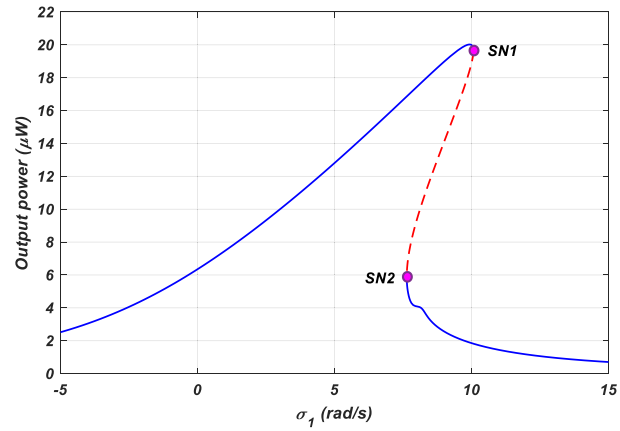

Fig. 5. Frequency response curve of the output power ($A = 0.5$ g, $\sigma_2 = 20$). Solid line: Stable solution, Dashed line: Unstable solution.

Fig. 5 depicts the frequency response of the output power of a harvester with $\sigma_2 = 20$ rad/s ($a = 2.4$ mm) excited in the vicinity of its first natural frequency ($f_1 = \omega_1/2\pi = 49.1$ Hz). The excitation is assumed to have an amplitude of $A = 0.5$ g and the impedance of the external load is chosen to match the impedance of the capacitor formed by the piezoelectric layers at the first natural frequency of the system ($R = 1/C_P\omega_1$). This impedance matching condition, if met, would lead to maximization of the output power of the harvester and has been used to calculate the load impedance in all the subsequent figures of the paper. As can be seen in Fig. 5, the frequency response is the same as one observed for a 1-DoF harvester with a duffing nonlinearity of the hardening type except for the small bump on the lower branch of the curve. There are two saddle–node bifurcation points indicated by $SN1$ and $SN2$ in the figure at which a stable node and a saddle point collide and annihilate each other. In the frequency interval between $SN1$ and $SN2$ the system has three equilibria including two stable nodes and one node with saddle stability. The trajectory passing through the saddle point in the phase-plane of the system defines the boundary between the attraction regions of each of the stable nodes. As the frequency approaches a bifurcation point, the saddle point moves toward one of these stable nodes leading to shrinkage of the attraction region corresponding to that node. This shrinkage continues until the saddle point collide the node at the bifurcation point, the node is annihilated and what remains is a single-stable vibratory system.

As the excitation amplitude increases the second mode of the system is excited through an internal resonance, contributes to the output power, and considerably changes the frequency response curves of the system. This effect is shown in Fig. 6.a and b where the excitation amplitude has been enhanced to $A = 0.8$ g and 1 g, respectively. The frequency responses of the system at the first and the second modes (a_1 and a_2) and the total output power of the harvester are depicted in this figure for both of the vibration amplitudes. It should be noted that while the amplitude of the second mode is considerably smaller than that of the first mode as shown in Fig. 6, its contributions to the power generation cannot be neglected due to two reasons. The first reason is the higher electromechanical coupling factor of the second mode χ_2 in comparison to that of the first mode χ_1 which occurs due to the larger slope of the second mode shape at the free end of the beam. The second reason is the appearance of ω_2^2 in the right hand of the expression in Eq. (48). Since the second mode is associated with a higher frequency (approximately three times the first one) the stored charges on the electrodes pass through the external

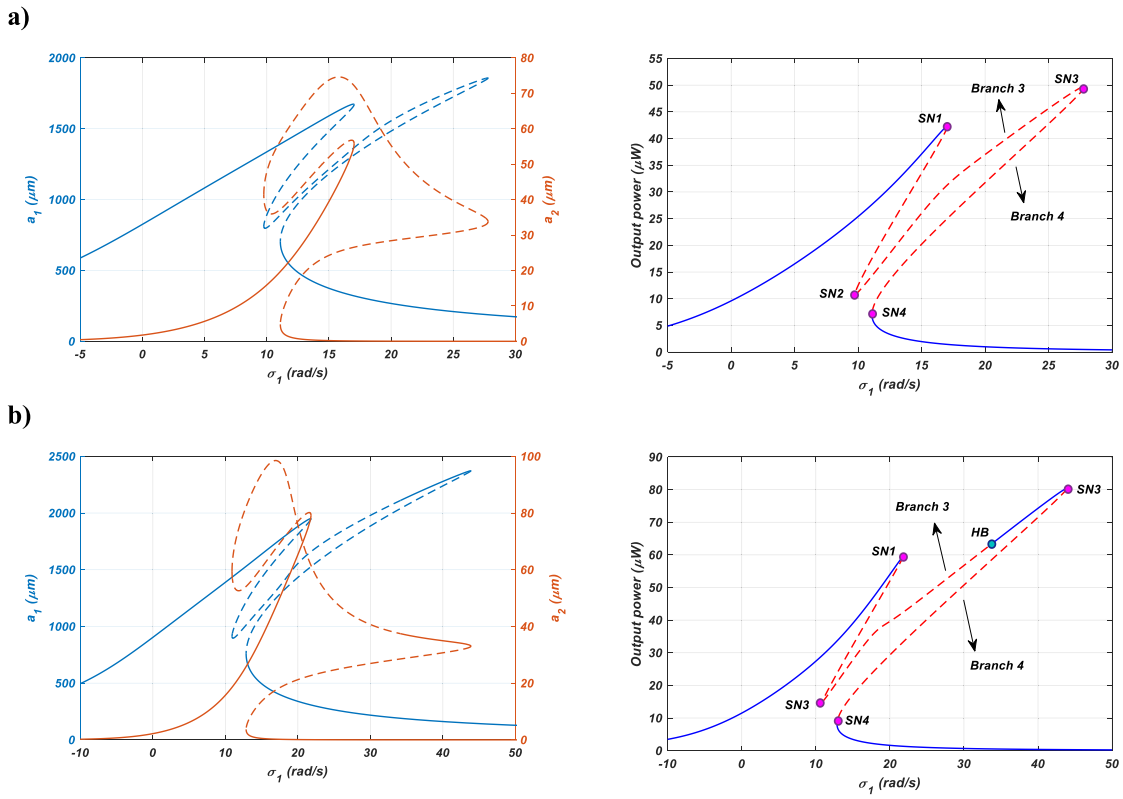

Fig. 6. Frequency response curves for the vibration amplitude at different modes and the total output power ($\sigma_2 = 20$). (a) $A = 0.8$ g (b) $A = 1$ g. Solid line: Stable solution, Dashed line: Unstable solution.

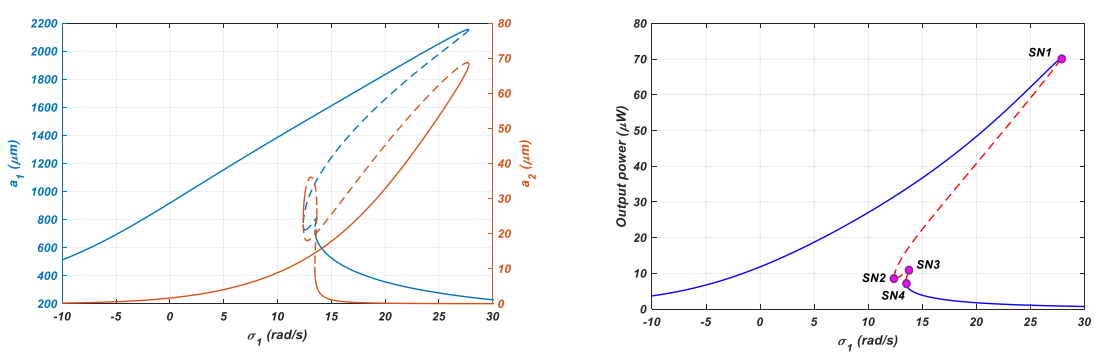

Fig. 7. Frequency response curves for the vibration amplitude at different modes and the total output power ($A = 1$ g, $\sigma_2 = 30$). Solid line: Stable solution, Dashed line: Unstable solution.

load more times during a specific time period leading to a higher power to be delivered to the load.

Comparison of Figs. 5 and 6 reveals that as the excitation amplitude enhances two new saddle–node bifurcation points appear where each one gives rise to a new branch of the solution (branches 3 and 4 in the figure). Although, these two branches correspond to unstable solutions in Fig. 6.a, as excitation amplitude is enhanced in Fig. 6.b some segment of branch 3 is switched to stable after emergence of a Hopf bifurcation point indicated by *HB* in the figure. Fig. 7 shows that as σ_2 further increases the bifurcation point $SN3$ moves toward lower frequencies making solution branches 3 and 4 shorter. That occurs while a decrease of σ_2 as evidenced by Fig. 8 results in the bifurcation points $SN1$ and *HB* to move toward lower frequencies and hence branches 1 and 2 get shorter and also the length of the stable segment on branch 3 increases. To verify the above-mentioned analytical findings, Eqs. (29) and (31) are also numerically solved employing the Runge–Kutta method and the obtained results are compared with those of the semi-analytical solution. The comparison is shown in Fig. 9 where both the analytical and numerical solutions are simultaneously depicted for $\sigma_2 = -5$ rad/s. To derive the numerical solution first the excitation frequency is ramped up smoothly in a step-wise fashion during a forward sweep and then through a backward sweep is ramped down again. The equations are numerically solved at each step given the steady state solution of the previous step as the initial condition. Consequently, the steady state voltage waveform is found and the instantaneous power delivered to the external load is calculated. Then this calculated power is averaged over time to give an approximate of the mean output power of the harvester. As can be seen in Fig. 9, the numerical solution surfs all the stable branches of the

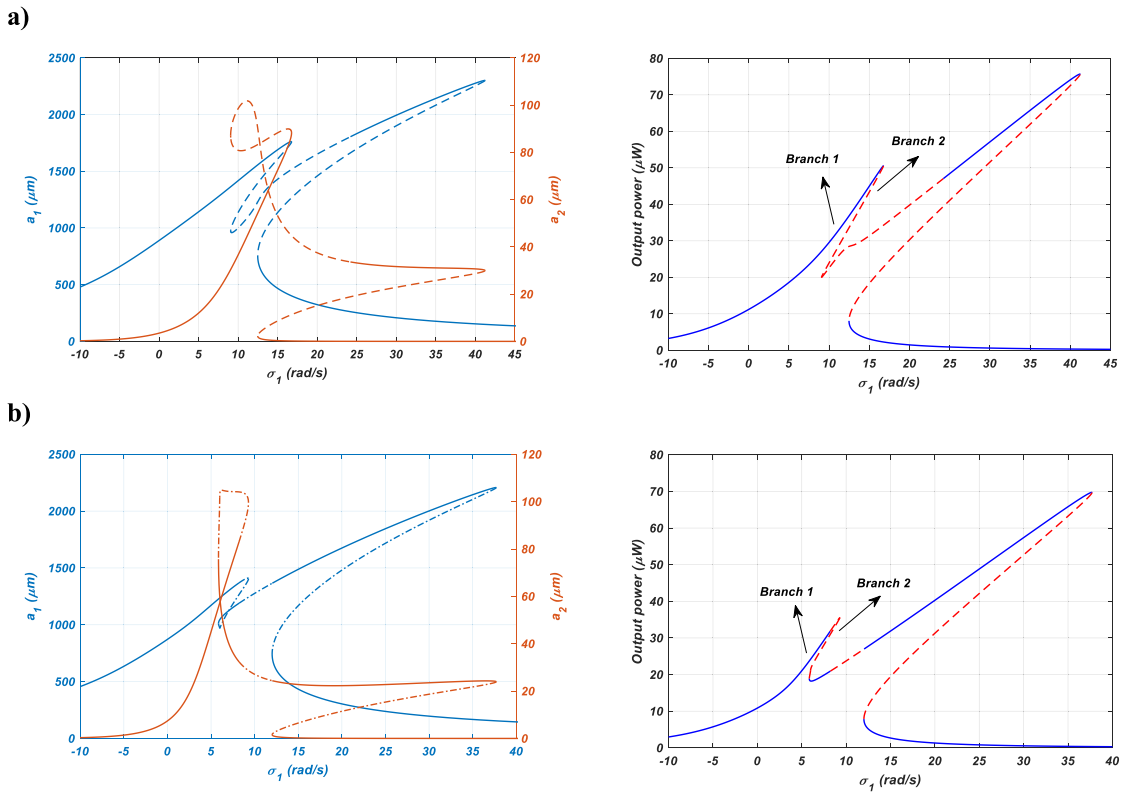

Fig. 8. Frequency response curves for the vibration amplitude at different modes and the total output power ($A = 1$ g). (a) $\sigma_2 = 10$ rad/s (b) $\sigma_2 = 0$. Solid line: Stable solution, Dashed line: Unstable solution.

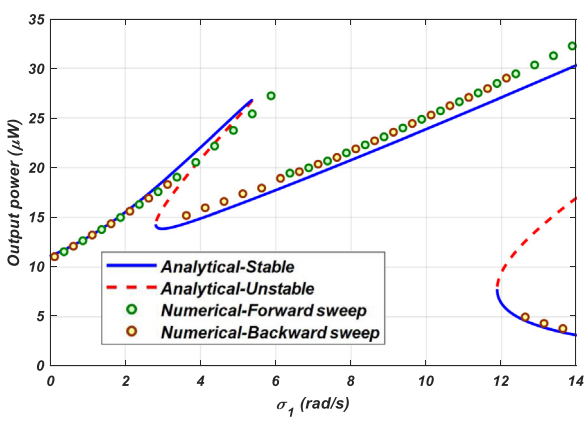

Fig. 9. Verification of the analytically-derived response curve using the numerical results ($A = 1$ g, $\sigma_2 = -5$ rad/s).

analytically-derived frequency response curve with an acceptable accuracy.

5. Conclusion

In this study, a two-mode model for a cantilever-type piezoelectric harvester is developed and employed to investigate the dynamic response and output power behavior of the device in both linear and nonlinear regimes. The nonlinear coupled electromechanical equations of the model are extracted through a comprehensive mathematical approach based on the Euler–Bernoulli assumptions. The equations are then order reduced by means of Galerkin's decomposition method with the mode shapes of the simple clamped-free beam used as the comparison functions. At small levels of excitation, the vibrational response at each mode may be treated separately where the excitation frequency determines whether and to what extent each mode is activated. Results indicate that in a system with a U-shaped attached mass, the natural frequencies remain closed to each other leading to enhancement of the output power through simultaneous engagement of both modes in environments with multi-frequency or wideband excitations. This is due to the fact that for a U-shaped mass unlike the simple cubic mass the inertial force and bending moment applied by the mass to the beam act in opposite directions. In the nonlinear regime an internal resonance would occur which couples the flexural modes and considerably alters the simple Duffing-type frequency response curve of the output power. As evidenced by the findings the response curves are composed of four branches, are bended toward higher frequencies, and contain both limit point and Hopf bifurcations. The emergence of a secondary peak adjacent to the primary one due to the internal resonance effect leads to further broadening of the effective bandwidth in a nonlinear harvester with coupled modes. Additionally, the second mode of the system due to its higher frequency and large electromechanical coupling parameter can considerably contribute to the output power when activated through the internal resonance. The extracted power calculated from the analytical approach is validated with a good agreement by a numerical solution.

CRediT authorship contribution statement

Abdolreza Pasharavesh: Conceptualization, Methodology, Investigation, Writing – original draft. **Hamid Dalir:** Writing – review & editing.

Declaration of competing interest

The authors declare that they have no known competing financial interests or personal relationships that could have appeared to influence the work reported in this paper.

Appendix A

The coefficients of the nonlinear terms appeared in Eq. (29) are as follows:

$$\alpha_{i1} = -D\int_0^L \left(\lambda_i'^2\ \lambda_i^{iv}\lambda_i + \lambda_i''^3\ \lambda_i + 4\lambda_i\lambda_i'\lambda_i''\lambda_i'''\right) dx$$

$$\alpha_{i2} = -D\int_0^L \left(2\lambda_i'\mu_i'\lambda_i^{iv}\lambda_i + \lambda_i'^2\ \mu_i^{iv}\lambda_i + 3\lambda_i''^2\ \mu_i''\lambda_i + 4\mu_i'\lambda_i''\lambda_i'''\lambda_i + 4\lambda_i'\mu_i''\lambda_i'''\lambda_i + 4\lambda_i'\lambda_i''\mu_i'''\lambda_i\right) dx$$

$$\alpha_{i3} = -D\int_0^L \left(\mu_i'^2\lambda_i^{iv}\lambda_i + 2\lambda_i'\mu_i'\mu_i^{iv}\lambda_i + 3\lambda_i''\ \mu_i''^2\lambda_i + 4\mu_i'\mu_i''\lambda_i'''\lambda_i + 4\mu_i'\lambda_i''\ \mu_i'''\lambda_i + 4\lambda_i'\ \mu_i''\mu_i'''\lambda_i\right) dx$$

$$\alpha_{i4} = -D\int_0^L \left(\mu_i'^2\mu_i^{iv}\lambda_i + \mu_i''^3\lambda_i + 4\mu_i'\mu_i''\mu_i'''\lambda_i\right) dx$$

$$\alpha_{i5} = \alpha_{i9} = m\int_0^L \left(\int_L^x \left(\int_0^x \lambda_i'^2\ dx\right) dx\right) \lambda_i'^2\ dx + M\left(\left(\int_0^L \lambda_i'^2\ dx\right) - a\left(\lambda_i'^2\right)\Big|_{x=L}\right)\int_0^L \lambda_i''\ \lambda_i dx$$

$$\alpha_{i6} = m\int_0^L \left(\int_L^x \left(\int_0^x \lambda_i'\ \mu_i' dx\right) dx\right) \lambda_i'^2\ dx + M\left(\left(\int_0^L \lambda_i'\ \mu_i' dx\right) + a\left(\lambda_i'\ \mu_i'\right)\Big|_{x=L}\right)\int_0^L \lambda_i''\ \lambda_i dx$$

$$\alpha_{i7} = m\int_0^L \left(\int_L^x \left(\int_0^x \lambda_i'\ \mu_i' dx\right) dx\right) \mu_i'\lambda_i'\ dx + M\left(\left(\int_0^L \lambda_i'\ \mu_i' dx\right) - a\left(\lambda_i'\ \mu_i'\right)\Big|_{x=L}\right)\int_0^L \mu_i''\ \lambda_i\ dx$$

$$\alpha_{i8} = \alpha_{i12} = m\int_0^L \left(\int_L^x \left(\int_0^x \mu_i'^2 dx\right) dx\right) \mu_i'\lambda_i'\ dx + M\left(\left(\int_0^L \mu_i'^2 dx\right) - a\left(\mu_i'^2\right)\Big|_{x=L}\right)\int_0^L \mu_i''\ \lambda_i\ dx$$

$$\alpha_{i10} = m\int_0^L \left(\int_L^x \left(\int_0^x \mu_i'^2 dx\right) dx\right) \lambda_i'^2\ dx + M\left(\left(\int_0^L \mu_i'^2 dx\right) - a\left(\mu_i'^2\right)\Big|_{x=L}\right)\int_0^L \lambda_i''\ \lambda_i dx$$

$$\alpha_{i11} = m\int_0^L \left(\int_L^x \left(\int_0^x \lambda_i'^2\ dx\right) dx\right) \mu_i'\lambda_i'\ dx + M\left(\left(\int_0^L \lambda_i'^2\ dx\right) - a\left(\lambda_i'^2\right)\Big|_{x=L}\right)\int_0^L \mu_i''\ \lambda_i\ dx$$

$$\alpha_{i13} = 2\alpha_{i6}, \qquad \alpha_{i14} = 2\alpha_{i7},$$

$$\alpha_{i15} = a_{i6} + a_{i11}, \qquad \alpha_{i16} = a_{i7} + a_{i10}$$

where:

$$i = 1, 2 \quad \lambda_1 = \mu_2 = \phi \qquad \lambda_2 = \mu_1 = \psi$$

Appendix B

The coefficients of the nonlinear terms appeared in Eq. (46) are as follows:

$$c_{11} = \begin{pmatrix} 3\left(\beta_1\alpha_{11} + \alpha_{24}\right) + 3\alpha_1\left(\beta_1\alpha_{12} + \alpha_{23}\right) \\ +3{\alpha_1}^2\left(\beta_1\alpha_{13} + \alpha_{22}\right) + 3{\alpha_1}^3\left(\beta_1\alpha_{14} + \alpha_{21}\right) \\ -3{\omega_1}^2\left(\beta_1\alpha_{15} + \alpha_{28}\right) \\ -3\alpha_1{\omega_1}^2\left(\beta_1\alpha_{16} + \alpha_{27}\right) - 3{\alpha_1}^2{\omega_1}^2\left(\beta_1\alpha_{17} + \alpha_{26}\right) \\ -3{\alpha_1}^3{\omega_1}^2\left(\beta_1\alpha_{18} + \alpha_{25}\right) + {\omega_1}^2\left(\beta_1\alpha_{19} + \alpha_{212}\right) \\ +{\omega_1}^2{\alpha_1}^2\left(\beta_1\alpha_{110} + \alpha_{211}\right) + {\omega_1}^2\alpha_1\left(\beta_1\alpha_{111} + \alpha_{210}\right) \\ +{\omega_1}^2{\alpha_1}^3\left(\beta_1\alpha_{112} + \alpha_{29}\right) + {\omega_1}^2\alpha_1\left(\beta_1\alpha_{113} + \alpha_{214}\right) \\ +{\omega_1}^2{\alpha_1}^2\left(\beta_1\alpha_{114} + \alpha_{213}\right) - 3\alpha_1{\omega_1}^2\left(\beta_1\alpha_{115} + \alpha_{216}\right) \\ -3{\alpha_1}^2{\omega_1}^2\left(\beta_1\alpha_{116} + \alpha_{215}\right) \end{pmatrix}$$

$$c_{12} = \begin{pmatrix} 6\left(\beta_1\alpha_{11} + \alpha_{24}\right) + \left(2\alpha_1 + 4\alpha_2\right)\left(\beta_1\alpha_{12} + \alpha_{23}\right) \\ + \left(2{\alpha_2}^2 + 4\alpha_1\alpha_2\right)\left(\beta_1\alpha_{13} + \alpha_{22}\right) \\ +6\alpha_1{\alpha_2}^2\left(\beta_1\alpha_{14} + \alpha_{21}\right) \\ - \left(2{\omega_1}^2 + 4{\omega_2}^2\right)\left(\beta_1\alpha_{15} + \alpha_{28}\right) - \left(2\alpha_1{\omega_1}^2 + 4\alpha_2{\omega_2}^2\right) \\ \left(\beta_1\alpha_{16} + \alpha_{27}\right) - \left(2{\alpha_2}^2{\omega_1}^2 + 4\alpha_1\alpha_2{\omega_2}^2\right)\left(\beta_1\alpha_{17} + \alpha_{26}\right) \\ - \left(2\alpha_1{\alpha_2}^2{\omega_1}^2 + 4\alpha_1{\alpha_2}^2{\omega_2}^2\right)\left(\beta_1\alpha_{18} + \alpha_{25}\right) \\ +2{\omega_2}^2\left(\beta_1\alpha_{19} + \alpha_{212}\right) + 2{\omega_2}^2{\alpha_2}^2\left(\beta_1\alpha_{110} + \alpha_{211}\right) \\ +2{\omega_2}^2\alpha_1\left(\beta_1\alpha_{111} + \alpha_{210}\right) + 2{\omega_2}^2\alpha_1{\alpha_2}^2\left(\beta_1\alpha_{112} + \alpha_{29}\right) \\ +2{\omega_2}^2\alpha_2\left(\beta_1\alpha_{113} + \alpha_{214}\right) + 2{\omega_2}^2\alpha_1\alpha_2\left(\beta_1\alpha_{114} + \alpha_{213}\right) \\ - \left(2\alpha_1{\omega_2}^2 + 2\alpha_2{\omega_2}^2 + 2\alpha_2{\omega_1}^2\right)\left(\beta_1\alpha_{115} + \alpha_{216}\right) \\ - \left(2\alpha_1\alpha_2{\omega_2}^2 + 2\alpha_1\alpha_2{\omega_1}^2 + 2{\alpha_2}^2{\omega_2}^2\right)\left(\beta_1\alpha_{116} + \alpha_{215}\right) \end{pmatrix}$$

$$c_{13} = \begin{pmatrix} 3\left(\beta_1\alpha_{11} + \alpha_{24}\right) + \left(\alpha_2 + 2\alpha_1\right)\left(\beta_1\alpha_{12} + \alpha_{23}\right) \\ + \left({\alpha_1}^2 + 2\alpha_1\alpha_2\right)\left(\beta_1\alpha_{13} + \alpha_{22}\right) + 3{\alpha_1}^2\alpha_2\left(\beta_1\alpha_{14} + \alpha_{21}\right) \\ - \left({\omega_2}^2 + 2{\omega_1}^2\right)\left(\beta_1\alpha_{15} + \alpha_{28}\right) - \left(\alpha_2{\omega_2}^2 + 2\alpha_1{\omega_1}^2\right) \\ \left(\beta_1\alpha_{16} + \alpha_{27}\right) - \left({\alpha_1}^2{\omega_2}^2 + 2\alpha_1\alpha_2{\omega_1}^2\right)\left(\beta_1\alpha_{17} + \alpha_{26}\right) \\ - \left({\alpha_1}^2\alpha_2{\omega_2}^2 + 2{\alpha_1}^2\alpha_2{\omega_1}^2\right)\left(\beta_1\alpha_{18} + \alpha_{25}\right) \\ + \left(2\omega_1\omega_2 - {\omega_1}^2\right)\left(\beta_1\alpha_{19} + \alpha_{212}\right) \\ + \left(2\alpha_1\alpha_2\omega_1\omega_2 - {\alpha_1}^2{\omega_1}^2\right)\left(\beta_1\alpha_{110} + \alpha_{211}\right) \\ + \left(2\alpha_1\omega_1\omega_2 - \alpha_2{\omega_1}^2\right)\left(\beta_1\alpha_{111} + \alpha_{210}\right) \\ + \left(2{\alpha_1}^2\alpha_2\omega_1\omega_2 - \alpha_1{}^2\alpha_2{\omega_1}^2\right)\left(\beta_1\alpha_{112} + \alpha_{29}\right) \\ + \left(\alpha_1\omega_1\omega_2 + \alpha_2\omega_1\omega_2 - \alpha_1{\omega_1}^2\right)\left(\beta_1\alpha_{113} + \alpha_{214}\right) \\ + \left({\alpha_1}^2\omega_1\omega_2 + \alpha_1\alpha_2\omega_1\omega_2 - \alpha_2\alpha_1{\omega_1}^2\right)\left(\beta_1\alpha_{114} + \alpha_{213}\right) \\ - \left({\omega_1}^2\alpha_1 + {\omega_1}^2\alpha_2 + {\omega_2}^2\alpha_1\right)\left(\beta_1\alpha_{115} + \alpha_{216}\right) \\ - \left({\alpha_1}^2{\omega_1}^2 + \alpha_1\alpha_2{\omega_1}^2 + \alpha_1\alpha_2{\omega_2}^2\right)\left(\beta_1\alpha_{116} + \alpha_{215}\right) \end{pmatrix}$$

$$c_{21} = \begin{pmatrix} 3\left(\beta_2\alpha_{11} + \alpha_{24}\right) + 3\alpha_2\left(\beta_2\alpha_{12} + \alpha_{23}\right) \\ +3{\alpha_2}^2\left(\beta_2\alpha_{13} + \alpha_{22}\right) + 3{\alpha_2}^3\left(\beta_2\alpha_{14} + \alpha_{21}\right) \\ -3{\omega_2}^2\left(\beta_2\alpha_{15} + \alpha_{28}\right) \\ -3\alpha_2{\omega_2}^2\left(\beta_2\alpha_{16} + \alpha_{27}\right) - 3{\alpha_2}^2{\omega_2}^2\left(\beta_2\alpha_{17} + \alpha_{26}\right) \\ -3{\alpha_2}^3{\omega_2}^2\left(\beta_2\alpha_{18} + \alpha_{25}\right) + {\omega_2}^2\left(\beta_2\alpha_{19} + \alpha_{212}\right) \\ +{\omega_2}^2{\alpha_2}^2\left(\beta_2\alpha_{110} + \alpha_{211}\right) + {\omega_2}^2\alpha_2\left(\beta_2\alpha_{111} + \alpha_{210}\right) \\ +{\omega_2}^2{\alpha_2}^3\left(\beta_2\alpha_{112} + \alpha_{29}\right) + {\omega_2}^2\alpha_2\left(\beta_2\alpha_{113} + \alpha_{214}\right) \\ +{\omega_2}^2{\alpha_2}^2\left(\beta_2\alpha_{114} + \alpha_{213}\right) - 3\alpha_2{\omega_2}^2\left(\beta_2\alpha_{115} + \alpha_{216}\right) \\ -3{\alpha_2}^2{\omega_2}^2\left(\beta_2\alpha_{116} + \alpha_{215}\right) \end{pmatrix}$$

$$c_{22} = \begin{pmatrix} 6\left(\beta_2\alpha_{11} + \alpha_{24}\right) + \left(2\alpha_2 + 4\alpha_1\right)\left(\beta_2\alpha_{12} + \alpha_{23}\right) \\ + \left(2{\alpha_1}^2 + 4\alpha_1\alpha_2\right)\left(\beta_2\alpha_{13} + \alpha_{22}\right) \\ +6{\alpha_1}^2\alpha_2\left(\beta_2\alpha_{14} + \alpha_{21}\right) \\ - \left(2{\omega_2}^2 + 4{\omega_1}^2\right)\left(\beta_2\alpha_{15} + \alpha_{28}\right) \\ - \left(2\alpha_2{\omega_2}^2 + 4\alpha_1{\omega_1}^2\right)\left(\beta_2\alpha_{16} + \alpha_{27}\right) \\ - \left(2{\alpha_1}^2{\omega_2}^2 + 4\alpha_1\alpha_2{\omega_1}^2\right)\left(\beta_2\alpha_{17} + \alpha_{26}\right) \\ - \left(2{\alpha_1}^2\alpha_2{\omega_2}^2 + 4{\alpha_1}^2\alpha_2{\omega_1}^2\right)\left(\beta_2\alpha_{18} + \alpha_{25}\right) \\ +2{\omega_1}^2\left(\beta_2\alpha_{19} + \alpha_{212}\right) + 2{\omega_1}^2{\alpha_1}^2\left(\beta_2\alpha_{110} + \alpha_{211}\right) \\ +2{\omega_1}^2\alpha_2\left(\beta_2\alpha_{111} + \alpha_{210}\right) + 2{\omega_1}^2{\alpha_1}^2\alpha_2\left(\beta_2\alpha_{112} + \alpha_{29}\right) \\ +2{\omega_1}^2\alpha_1\left(\beta_2\alpha_{113} + \alpha_{214}\right) + 2{\omega_1}^2\alpha_1\alpha_2\left(\beta_2\alpha_{114} + \alpha_{213}\right) \\ - \left(2\alpha_1{\omega_1}^2 + 2\alpha_2{\omega_1}^2 + 2\alpha_1{\omega_2}^2\right)\left(\beta_2\alpha_{115} + \alpha_{216}\right) \\ - \left(2{\alpha_1}^2{\omega_1}^2 + 2\alpha_1\alpha_2{\omega_1}^2 + 2\alpha_1\alpha_2{\omega_2}^2\right)\left(\beta_2\alpha_{116} + \alpha_{215}\right) \end{pmatrix}$$

$$c_{23} = \begin{pmatrix} (\beta_2\alpha_{11} + \alpha_{24}) + \alpha_1 (\beta_2\alpha_{12} + \alpha_{23}) + {\alpha_1}^2 (\beta_2\alpha_{13} + \alpha_{22}) \\ +{\alpha_1}^3 (\beta_2\alpha_{14} + \alpha_{21}) - {\omega_1}^2 (\beta_2\alpha_{15} + \alpha_{28}) \\ -\alpha_1{\omega_1}^2 (\beta_2\alpha_{16} + \alpha_{27}) - {\alpha_1}^2{\omega_1}^2 (\beta_2\alpha_{17} + \alpha_{26}) \\ -{\alpha_1}^3{\omega_1}^2 (\beta_2\alpha_{18} + \alpha_{25}) - {\omega_1}^2 (\beta_2\alpha_{19} + \alpha_{212}) \\ -{\alpha_1}^2{\omega_1}^2 (\beta_2\alpha_{110} + \alpha_{211}) - \alpha_1{\omega_1}^2 (\beta_2\alpha_{111} + \alpha_{210}) \\ -{\alpha_1}^3{\omega_1}^2 (\beta_2\alpha_{112} + \alpha_{29}) - \alpha_1{\omega_1}^2 (\beta_2\alpha_{113} + \alpha_{214}) \\ -{\alpha_1}^2{\omega_1}^2 (\beta_2\alpha_{114} + \alpha_{213}) - \alpha_1{\omega_1}^2 (\beta_2\alpha_{115} + \alpha_{216}) \\ -{\alpha_1}^2{\omega_1}^2 (\beta_2\alpha_{116} + \alpha_{215}) \end{pmatrix}$$

References

Chung, G.-S., Lee, B.-C., 2014. Fabrication and characterization of vibration-driven AlN piezoelectric micropower generator compatible with complementary metal-oxide semiconductor process. J. Intell. Mater. Syst. Struct. 1045389X14546649.

Erturk, A., 2012. Assumed-modes modeling of piezoelectric energy harvesters: Euler–Bernoulli, Rayleigh, and timoshenko models with axial deformations. Comput. Struct. 106, 214–227.

Erturk, A., Inman, D.J., 2008. A distributed parameter electromechanical model for cantilevered piezoelectric energy harvesters. J. Vib. Acoust. 130, 041002.

Green, P.L., Papatheou, E., Sims, N.D., 2013. Energy harvesting from human motion and bridge vibrations: An evaluation of current nonlinear energy harvesting solutions. J. Intell. Mater. Syst. Struct. 24, 1494–1505.

Hajati, A., Kim, S.-G., 2011. Ultra-wide bandwidth piezoelectric energy harvesting. Appl. Phys. Lett. 99, 083105.

Hande, A., Bridgelall, R., Bhatia, D., 2009. Energy harvesting for active RF sensors and ID tags. In: Energy Harvesting Technologies. Springer, pp. 459–492.

Hu, H., Dai, L., Chen, H., Jiang, S., Wang, H., Laude, V., 2017. Two methods to broaden the bandwidth of a nonlinear piezoelectric bimorph power harvester. J. Vib. Acoust. 139, 031008.

Jiang, S., Li, X., Guo, S., Hu, Y., Yang, J., Jiang, Q., 2005. Performance of a piezoelectric bimorph for scavenging vibration energy. Smart Mater. Struct. 14, 769.

Lumentut, M.F., Howard, I.M., 2016. Parametric design-based modal damped vibrational piezoelectric energy harvesters with arbitrary proof mass offset: numerical and analytical validations. Mech. Syst. Signal Process. 68, 562–586.

Lumentut, M., Howard, I., 2017. Intrinsic electromechanical dynamic equations for piezoelectric power harvesters. Acta Mech. 228, 631–650.

Mahmoodi, S.N., Afshari, M., Jalili, N., 2008. Nonlinear vibrations of piezoelectric microcantilevers for biologically-induced surface stress sensing. Commun. Nonlinear Sci. Numer. Simul. 13, 1964–1977.

Mallick, D., Amann, A., Roy, S., 2016. Surfing the High Energy output Branch of Nonlinear energy harvesters. Phys. Rev. Lett. 117, 197701.

Mann, B., Sims, N., 2009. Energy harvesting from the nonlinear oscillations of magnetic levitation. J. Sound Vib. 319, 515–530.

Masana, R., Daqaq, M.F., 2011. Electromechanical modeling and nonlinear analysis of axially loaded energy harvesters. J. Vib. Acoust. 133, 011007.

Masuda, A., Sato, T., 2016. Global stabilization of high-energy resonance for a nonlinear wideband electromagnetic vibration energy harvester. In: Active and Passive Smart Structures and Integrated Systems 2016. International Society for Optics and Photonics, p. 97990K.

Miao, P., Mitcheson, P., Holmes, A., Yeatman, E., Green, T., Stark, B., 2006. MEMS inertial power generators for biomedical applications. Microsyst. Technol. 12, 1079–1083.

Panyam, M., Daqaq, M.F., 2016. A comparative performance analysis of electrically optimized nonlinear energy harvesters. J. Intell. Mater. Syst. Struct. 27, 537–548.

Pasharavesh, A., Ahmadian, M.T., 2018. Analytical and numerical simulations of energy harvesting using MEMS devices operating in nonlinear regime. Eur. Phys. J. B 91, 241.

Pasharavesh, A., Ahmadian, M., 2020. Toward Wideband Piezoelectric Harvesters through self-powered transitions to high-energy response. J. Vib. Acoust. 142.

Pasharavesh, A., Ahmadian, M., Zohoor, H., 2017. On the energy extraction from large amplitude vibrations of MEMS-based piezoelectric harvesters. Acta Mech. 1–24.

Pasharavesh, A., Ahmadian, M., Zohoor, H., 2019. Complex modal analysis and coupled electromechanical simulation of energy harvesting piezoelectric laminated beams. Proc. Inst. Mech. Eng. C 233, 2526–2537.

Pasharavesh, A., Moheimani, R., Dalir, H., 2020a. Nonlinear energy harvesting from vibratory disc-shaped piezoelectric laminates. Theor. Appl. Mech. Lett. 10, 253–261.

Pasharavesh, A., Moheimani, R., Dalir, H., 2020b. Performance analysis of an Electromagnetically Coupled Piezoelectric Energy Scavenger. Energies 13, 845.

Quinn, D.D., Triplett, A.L., Bergman, L.A., Vakakis, A.F., 2011. Comparing linear and essentially nonlinear vibration-based energy harvesting. J. Vib. Acoust. 133, 011001.

Rao, S.S., 2007. Vibration of Continuous Systems. John Wiley & Sons.

Sheu, G.-J., Yang, S.-M., Lee, T., 2011. Development of a low frequency electrostatic comb-drive energy harvester compatible to SoC design by CMOS process. Sensors Actuators A 167, 70–76.

Singh, K.A., Kumar, R., Weber, R.J., 2015. A broadband bistable Piezoelectric energy harvester with nonlinear high-power extraction. IEEE Trans. Power Electron. 30, 6763–6774.

Stanton, S.C., Erturk, A., Mann, B.P., Inman, D.J., 2010. Nonlinear piezoelectricity in electroelastic energy harvesters: modeling and experimental identification. J. Appl. Phys. 108, 074903.

Wang, P., Tanaka, K., Sugiyama, S., Dai, X., Zhao, X., Liu, J., 2009. A micro electromagnetic low level vibration energy harvester based on MEMS technology. Microsyst. Technol. 15, 941–951.

Yang, J., 2005. An Introduction to the Theory of Piezoelectricity. Springer Science & Business Media.

Yu, H., Zhou, J., Deng, L., Wen, Z., 2014. A vibration-based mems piezoelectric energy harvester and power conditioning circuit. Sensors 14, 3323–3341.

Zhou, S., Cao, J., Inman, D.J., Liu, S., Wang, W., Lin, J., 2015. Impact-induced high-energy orbits of nonlinear energy harvesters. Appl. Phys. Lett. 106, 093901.